Inhibition of PAK2 in endothelial cells suppresses tumor angiogenesis and promotes immune sensitization through CXCL10 expression

Jeanne Corriveau[1], Pascale Monot[1], Chantal Delisle[1], Marie-Anne Goyette[2], Yassine El Bakkouri[1], Trang Hoang[1, 3], Jean-François Côté[2, 4, 5], Jean-Philippe Gratton[1]†

1 Department of Pharmacology and Physiology, Faculty of Medicine, Université de Montréal, Montreal, Quebec, Canada

2 Montreal Clinical Research Institute (IRCM), Montreal, Quebec, Canada

3 Institute of Research in Immunology and Cancer (IRIC), Université de Montréal, Montreal, Quebec, Canada

4 Department of Anatomy and Cell Biology, McGill University, Montreal, Quebec, Canada

5 Department of Medicine, Faculty of Medicine, Université de Montréal, Montreal, Quebec, Canada

† Author for correspondence: jean-philippe.gratton@umontreal.ca

Keywords: PAK2, CXCL10, tumor angiogenesis, tumor immunity, tumor microenvironment

ABSTRACT

Tumor angiogenesis is essential for the growth of solid tumors. This process is characterized by an increased secretion of pro-angiogenic factors and results in a disorganized tumor vasculature. It has been shown that the protein p21-activated kinase 2 (PAK2) is involved in the intracellular signaling cascades of pro-angiogenic factors leading to endothelial cell (EC) migration and lumen formation, all essential steps of physiological angiogenesis. However, the involvement of PAK2 in tumor angiogenesis remains ill-defined. Here, we show that, during orthotopic tumor growth, the specific deletion of *PAK2* in ECs reduces tumor size and tumor angiogenesis. In addition, endothelial-specific loss of PAK2 was found to normalize the remaining tumor blood vessels, favoring innate immune cells infiltration within tumors. Importantly, we uncovered a role for PAK2 in regulating chemokine expression, notably C-X-C motif chemokine 10 (CXCL10). Secretion of CXCL10 is enhanced following PAK2 depletion in ECs. Furthermore, we show that CXCL10 is essential for the effects induced by the deletion of PAK2 on tumor vasculature and immune composition of tumors. Together, our findings identify PAK2 inhibition in tumor ECs as a potential target to reduce tumor angiogenesis and reprogram ECs to promote immune cell infiltration within tumors through the expression of CXCL10.

INTRODUCTION

The tumor microenvironment (TME), the ecosystem in which tumors develop, plays an active role in the pathogenesis of cancer as it influences both neoplasia progression and the response to therapy (1). In addition to the primary cancer cells that form the bulk of the tumor, a wide variety of non-cancerous cells, including endothelial cells (ECs), fibroblasts, and immune cells compose the TME. ECs contribute to tumor angiogenesis, the formation of new blood vessels that supply nutrients and oxygen to the tumor (2). Tumor vascularization is essential for the growth of solid tumors as non-vascularized tumors do not grow more than a few millimeters in diameters (2,3). Indeed, as a tumor grows, cancer cells become hypoxic, leading to their reprogramming to express pro-angiogenic factors, such as hypoxia-inducible factors (HIFs), vascular endothelial growth factor (VEGF), platelet-derived growth factor (PDGF), angiopoietins and other cytokines, that collectively operate to initiate neo-angiogenesis to meet their metabolic needs (4,5). However, due to the unbalanced increase of pro-angiogenic factors, tumor blood vessels exhibit an immature phenotype compared to vessels in normal tissues (6,7). Tumor vessels are excessively branched, chaotic and leaky, as they lack pericyte and smooth muscle coverage, and possess an inconsistent basement membrane with irregular endothelial lining. This phenotype leads to inconsistent perfusion and a hypoxic tumor state, contributing to the sustained secretion of pro-angiogenic factors (6).

Hypoxia also contributes to the chronic inflammatory state of tumors, which is an essential component of the TME and one of the hallmarks of cancer (8). Hypoxia leads to the upregulation of pro-inflammatory cytokines and C-C and C-X-C chemokines that promote the recruitment of immune cells, such as macrophages, neutrophils, and lymphocytes, to the hypoxic regions of the tumor (9). These recruited cells directly contribute to the accentuation of tumor blood vessels abnormalities by releasing pro-angiogenic factors in the TME (10). In addition, inflammatory

cytokines and chemokines can promote the recruitment of immunosuppressive cells, such as tumor-associated macrophages and regulatory T cells (Tregs), and inhibit the function of cytotoxic T cells and natural killer (NK) cells, that collectively contributes to immune suppression and immune evasion (11). C-C and C-X-C chemokines also play important roles in tumor angiogenesis, having either angiogenic or angiostatic effects (12). For instance, CXCL8, CXCL12, CCL2, and CCL5 promote the migration and proliferation of ECs, while CXCL4, CXCL9, CXCL10 and CXCL14 inhibit these processes (12,13). CXCL10 expression in the TME is generally associated with anti-tumor effects through immunogenic and angiostatic activities, although its expression has also been associated with tumor progression in certain types of cancer (14). Combining anti-angiogenic agents with immunotherapy has been proposed to improve treatment efficacy (15). However, anti-angiogenic agents, mostly targeting the VEGF-signaling pathways, have encountered therapeutic resistance in the clinic, partly due to the activation of alternative pro-angiogenic pathways (16).

p21-activated kinases (PAKs) are serine/threonine kinase best known to be effectors of the small Rho GTPases of the Rac- and Cdc42-subfamillies. The PAK family is divided into Group I (PAK1, 2, 3) and Group II (PAK4, 5, 6), and is involved in various cellular processes, including cytoskeletal remodeling, cell motility, proliferation and survival (17). Among Group I PAKs, PAK2 is ubiquitously expressed, whereas the expressions of PAK1 and PAK3 exhibit tissue specificity (18). PAK1, 2 and 4 are expressed in vascular tissues, with PAK2 being the dominant PAK isoform expressed in ECs (18,19). PAK1-deficient mice are viable and fertile with minor immune, neuronal and glucose homeostasis defects (20). PAK4-deficient mice show heart and neuronal defects and lack vascular branching leading to embryonic lethality, but specific deletion of PAK4 in ECs of adult mice did not affect normal endothelial functions (20,21). In contrast, PAK2 knockout (KO) mice, as well as mice with endothelial-specific depletion of PAK2, are embryonic lethal due to

vascular defects including impaired vascular remodeling and altered barrier function (20,22,23). In adult mice, induction of global *PAK2* genetic deletion is also lethal and the induction of endothelial-specific depletion results in increased vascular permeability in various tissues (23). In ECs, PAK2 activation is necessary for VEGF- and angiopoietin-1-stimulated migration and angiogenic sprouting (23-25). Interestingly, endothelial-specific deletion of PAK4 in mice inhibited angiogenesis and growth of glioblastoma tumors (21). Surprisingly, despite being the dominant isoform expressed in ECs, the role of PAK2 in tumor angiogenesis remains ill-defined.

Here, we report that induction of endothelial-specific deletion of *PAK2* during the growth of orthotopic tumors in mice results in reduced tumor size and angiogenesis, and induced the normalization of tumor blood vessels. Notably, deletion of PAK2 in ECs increases the presence of innate immune cells into tumors, in particular NK and dendritic cells (DCs), and results in augmented expression of chemokines, including CXCL10. Importantly, neutralization of CXCL10 with blocking antibodies reverses the anti-tumor effects induced by PAK2 deletion. Together, our findings show that the endothelial-specific deletion of PAK2 in tumors inhibits tumor angiogenesis and reprograms ECs to promote, in a CXCL10-dependent manner, immune cell infiltration limiting tumor progression.

RESULTS

Conditional deletion of PAK2 in tumor ECs suppresses tumor angiogenesis and growth

The goal of this study is to define the contributions of PAK2 to tumor angiogenesis. Since endothelial-specific loss of PAK2 induces lethality during mouse embryonic development (23), we generated a mouse line that allowed us to induce endothelial *Pak2* gene deletion in adult mice upon tamoxifen treatment to determine the functions of PAK2 in tumor blood vessels. Pak2$^{fl/fl}$ mice (23), were crossed with Pdgfb-iCreER mice (26) to generate Pdgfb-iCreER;Pak2$^{fl/fl}$ mice which were viable and fertile with no obvious phenotypes. Pdgfb-iCreER;Pak2$^{fl/fl}$ mice were genotyped by PCR analysis (Figure S1A). To validate this model, we confirmed that tamoxifen treatment of Pdgfb-iCreER;Pak2$^{fl/fl}$ mice resulted in deletion of PAK2 in ECs of mice (KO-PAK2^{EC}). PAK2$^{fl/fl}$ mice treated with tamoxifen (CT-PAK2^{EC}), or Pdgfb-iCreER;Pak2$^{fl/fl}$ treated with a placebo (PCB-PAK2^{EC}) were used as controls (Figure 1A). To verify the efficiency of PAK2 protein loss in cells, mouse lung ECs (MLECs) were isolated from Pdgfb-iCreER;Pak2$^{fl/fl}$ mice and treated with increasing concentrations of 4-hydroxytamoxifen (OH-tamoxifen) for 24 h *ex vivo*. As predicted, MLECs isolated from Pdgfb-iCreER;Pak2$^{fl/fl}$ mice and treated with OH-tamoxifen showed a significant reduction in PAK2 protein levels (Figure S1B).

In order to determine if the loss of PAK2 in ECs affects tumor angiogenesis, Lewis Lung Carcinoma (LLC) tumor cells were injected subcutaneously into the flank of KO-PAK2^{EC}, CT-PAK2^{EC} or PCB-PAK2^{EC} mice. Tumors were allowed to grow for a maximum of 18 days and tumor size was measured daily (Figure 1A). The growth of tumors on KO-PAK2^{EC} mice was significantly reduced compared to tumors on CT-PAK2^{EC} or PCB-PAK2^{EC} mice (Figure 1B). The endothelial-specific loss of PAK2 within the tumor vasculature of KO-PAK2^{EC} mice was confirmed by CD31

and PAK2 immunofluorescence staining of tumor tissue sections. Tumor isolated from KO-PAK2^{EC} showed absence of CD31 and PAK2 colocalization in contrast to staining in CT-PAK2^{EC} tumors, while PAK2 staining outside tumor ECs remained unaffected (Figure 1C). To assess the effect of endothelial PAK2 loss on tumoral vascularization, the CD31-positive area was quantified by immunofluorescence staining of tumor tissue sections. KO-PAK2^{EC} tumors had less CD31 staining, an EC marker, compared to tumors implanted on CT-PAK2^{EC} or on PCB-PAK2^{EC} (Figure 1D). Due to the lack of significant differences between control groups in tumor growth or levels of intra-tumoral vascularization, we elected to use CT-PAK2^{EC} mice (Pak2$^{fl/fl}$ + Tamoxifen) as our main control group for further experiments. Overall, these results show that the endothelial-specific deletion of PAK2 reduces both tumor growth and tumor vascularization, demonstrating an essential role for endothelial PAK2 in the TME in determining tumor progression and angiogenesis.

A hallmark of tumor angiogenesis is an immature and disorganized vasculature (6). We, therefore, investigated if the loss of PAK2 expression in tumor ECs affects the structural and functional states of tumor blood vessels. Despite the overall reduced tumoral vascularization, the blood vessels found in KO-PAK2^{EC} tumors were of larger caliber, showing more vascular structures of wider diameter (> 10 μm), than the blood vessels found in CT-PAK2^{EC} tumors (Figure 1E, IF). KO-PAK2^{EC} tumor blood vessels also possess higher pericyte coverage compared to control tumors, with increased levels of the pericyte marker NG2 relative to CD31 levels in tumors (Figure 1G). Since these results suggested that the blood vessels in KO-PAK2^{EC} tumors were better supported by pericytes and more stable, we examined the extent of their leakiness to fibrinogen. KO-PAK2^{EC} tumors had a decreased extravascular deposition of fibrinogen compared to CT-PAK2^{EC} tumors (Figure 1H), indicating that KO-PAK2^{EC} tumor blood vessels are less permeable to macromolecule extravasation. Altogether, these results show that the deletion of PAK2 in ECs suppresses tumor

angiogenesis, reducing both tumor growth and vascularization, and leads to normalization of tumor blood vessels.

KO-PAK2^{EC} tumors express an immune response gene signature

To gain insights into the consequences of endothelial PAK2 deletion on tumors, we performed RNA-sequencing (RNA-seq) analysis of three KO-PAK2^{EC} and three CT-PAK2^{EC} tumors. Differential gene expression analyses identified 478 upregulated and 166 downregulated transcripts in KO-PAK2^{EC} tumors compared to CT-PAK2^{EC} tumors (Figure 2A and Table S1). Melanoma antigen family A10 (*MAGEA10*) was the most upregulated gene in KO-PAK2^{EC} tumors (Fold increase = 61.5) while Transmembrane Serine Protease 11B (*TMPRSS11B*) was the most downregulated gene (Fold decrease = -4.1). Cadherin 9 (*CDH9*), lymphocyte antigen 6 complex locus G (*LY6G*), Rab17 (*RAB17*) and bone morphogenetic protein 5 (*BMP5*) were amongst the top 10% of upregulated genes and Rab15 (*RAB15*) and Collagen Type XXIII Alpha 1 Chain (*COL23A1*) in the top 10% of downregulated genes in KO-PAK2^{EC} tumors (Table S1, Figure 2A). Differential gene expression of selected transcripts was confirmed by RT-qPCR (Figure S2A). Gene ontology (GO) analysis centered on biological processes of the 644 differentially expressed genes (DEGs) in KO-PAK2^{EC} tumors identified numerous significant GO annotations (Table S2). Interestingly, many of the top 20 most significant GO annotations of DEGs in KO-PAK2^{EC} tumors were associated to an activation of the immune response, such as defense response (GO:0006952), innate immune response (GO:0045087), response to interferon-beta (GO:0035456), immune response (GO:0006955) and response to interferon-gamma (GO:0034341) (Figure 2B). Gene set enrichment analysis (GSEA) confirmed that the immune response gene set (GO:0006955) was enriched in KO-PAK2^{EC} tumors compared to CT-PAK2^{EC} tumors (Figure 2C). In contrast, the sprouting angiogenesis gene set (GO:0002040) was enriched in CT-PAK2^{EC} tumors, consistent

with the reduction in vascularization levels we observed in KO-PAK2^{EC} tumors (Figure 2D). Regulation of programmed cell death (GO:0043067), inflammatory response (GO:0006954) and response to cytokine (GO:0034097) gene sets were also enriched in KO-PAK2^{EC} tumors compared to CT-PAK2^{EC} tumors (Figure S2B-D). These analyses strongly suggest that KO-PAK2^{EC} tumors are more immunologically active than CT-PAK2^{EC} tumors. Furthermore, analysis of all the significant GO annotations identified (Table S2) revealed that many of them are associated with the response to cytokines, adhesion and chemotaxis of immune cells (Figure 2E). Leukocyte cell-cell adhesion (GO:0007159) and leukocyte chemotaxis (GO:0030595) gene sets were significantly enriched in KO-PAK2^{EC} tumors (Figure 2F, G). Taken together, these analyses reveal that the conditional loss of PAK2 in ECs rewires the transcriptomic profile of KO-PAK2^{EC} tumors, resulting in a microenvironment that may promote the infiltration of immune cells.

Deletion of PAK2 in tumoral ECs enhances innate immune cell infiltration

To assess the possibility that endothelial deletion of PAK2 triggers an immune response in tumors, we determined the immune cell profiles of KO-PAK2^{EC} and CT-PAK2^{EC} tumors by multiparametric flow cytometry analysis. These analyses showed a significant increase in the presence and/or infiltration of DCs, migratory CD103^{+} DCs, NK cells and activated CD44^{+} NK cells, all innate immune cell types, in KO-PAK2^{EC} tumors (Figure 3A). We next investigated the localization of these immune cells within the tumor by immunohistochemical staining. Hematoxylin counterstain was used to determine core and periphery regions (Figure S3A). Immunohistochemical staining of CD11c and NK1.1 showed that KO-PAK2^{EC} tumors had more DCs and NK cells in the core regions of tumors (Figure 3B, D) while no significant difference was observed at the periphery of tumors (Figure 3C, E). No significant difference in the content of adaptative immune cells was observed by flow cytometry analysis in KO-PAK2^{EC} and CT-PAK2^{EC} tumors (Figure 3A). However,

immunostaining of KO-PAK2^{EC} tumors revealed that they had less CD4^{+} T cells at their periphery than CT-PAK2^{EC} tumors, but no difference was observed in the core regions of tumors (Figure S3B, C). No difference was observed for CD8^{+} T cells in the core or periphery of tumors (Figure S3D, E).

To determine if the immune transcriptomic changes observed in KO-PAK2^{EC} tumors are consistent with increased infiltration of innate immune cells, we further interrogated the DEGs between KO-PAK2^{EC} and CT-PAK2^{EC} tumors that are involved in the immune response gene set (GO:0006955) (Figure S2E). Analysis of these 108 DEGs using Gene ontology centered on biological process revealed that the GO term innate immune response (GO:0045087) was more significantly enriched than the GO term adaptative immune response (GO:0002250) (Figure S2F). In addition, pathway analysis using the KEGG database revealed that these genes were also enriched in pathways mostly involved in innate immune response such as NOD-like receptor signaling, C-type lectin receptor signaling and cytosolic DNA-sensing pathways, and pro-inflammatory cytokine responses, including IL-17 signaling, TNF signaling and NF-kappa B signaling pathways (Figure S2G). Altogether, these results demonstrate that KO-PAK2^{EC} tumors had increased innate immune cell infiltration, principally DCs and NK cells.

Inhibition of PAK2 in ECs increases the expression of the chemokine CXCL10

To determine how PAK2 expression in ECs could affect the immune cell content of tumors, we compared the transcriptomes of control and PAK2-depleted human umbilical vein ECs (HUVECs). Bulk RNA-seq was carried out on HUVECs transfected with either control (siCT) or siRNA targeting PAK2 (siPAK2). The PAK2 protein expression level was downregulated by more than 85% in siPAK2 transfected cells (Figure S4A). We identified 1521 DEGs (986 upregulated and 535

downregulated genes) in siPAK2 compared to siCT transfected HUVECs (Figure 4A and Table S3). As anticipated, *PAK2* was found among the most downregulated DEGs (Fold decrease = -4.8). The downregulation of PAK2 did not significantly affect the differential expression of other PAK genes (*PAK1*, *3*, *4*, *5*, *6*) (Figure S4B, C). Interestingly, among the top 20 upregulated DEGs in siPAK2 transfected HUVECs four of them were chemokines: *CXCL10* (Fold increase = 30.7), *CX3CL1* (Fold increase = 16.7), *CXCL11* (Fold increase = 14.9) and *CXCL12* (Fold increase = 11.4) (Fig. 4B and Table S3). This prompted us to search for chemokine-related gene enrichment in the transcriptome of PAK2-downregulated HUVECs. GSEA analysis showed strong enrichment of the Chemokine production (GO:0032602) and Chemokine-mediated signaling pathway (GO:0070098) gene sets in siPAK2 transfected cells (Figure 4C and S4D). In total, fourteen DEGs coding for chemokines were identified (Figure 4D). Except for *CCL14*, which was downregulated, all the other chemokines were upregulated in PAK2-depleted HUVECs (Figure 4D). The differential expression of these chemokines was validated by RT-qPCR (Figure 4E). Similar to the bulk RNA-seq data, levels of *CXCL10* mRNA were the most upregulated (Fold increase = 37.0) (Figure 4D, E).

Next, to determine if PAK2 kinase activation is necessary for the induction of chemokines, we inhibited PAK2 in HUVECs with a pharmacological inhibitor of group I PAKs, FRAX1036 (27), and showed that it also caused an augmentation of *CXCL10* mRNA levels (Figure 4F). Upregulation of other chemokines was also observed in HUVECs following FRAX1036 treatment (Figure S4E). Inhibition of PAK2 activity by FRAX1036 was confirmed by the reduction in the levels of Ser-141 phosphorylation on PAK2 (Figure 4F). Importantly, depletion of PAK2 increased the expression of the CXCL10 protein in HUVECs (Figure 4G). CXCL10 levels were also markedly increased in the cell culture medium of siPAK2-tranfected HUVECs (Figure 4G). These

results suggest that inhibition of PAK2 in ECs increases the immunological response by stimulating the expression and production of chemokines by ECs, in particular of CXCL10.

Expression of CXCL10 is increased in KO-PAK2^{EC} tumors

Subsequently, we examined if the expression levels of some of the aforementioned chemokines were also increased in tumors from KO-PAK2^{EC} mice. Bulk RNA-seq data of KO-PAK2^{EC} tumors revealed that three genes coding for chemokines (*CXCL1*, *CXCL2* and *CXCL10*) were identified among DEGs (Table S1). Similar to the RNA-seq data from PAK2-depleted ECs (Figure 4), *CXCL10* had the highest fold change expression (Fold increase = 2.3) in tumors in which endothelial PAK2 expression was suppressed (Figure 5A). The upregulation of *CXCL10* mRNA was confirmed by RT-qPCR in KO-PAK2^{EC} tumors (Figure S2B). To assess CXCL10 protein levels and its localization relative to tumor blood vessels, CT-PAK2^{EC} and KO-PAK2^{EC} tumor sections were stained for CXCL10 and CD31 by immunofluorescence (Figure 5B). KO-PAK2^{EC} tumors showed more CXCL10-positive signal per area than CT-PAK2^{EC} tumors, confirming CXCL10 upregulation at the protein level (Fig 5C). However, for both tumor groups CXCL10 signals were located in proximity to CD31-positive structures and no difference in the distances between the CXCL10 signal clusters and tumor ECs was observed in KO-PAK2^{EC} and CT-PAK2^{EC} tumors (Fig 5D). Overall, these results indicate that CXCL10 production is increased in PAK2-depleted tumors ECs.

Neutralization of CXCL10 abolishes endothelial PAK2 deletion-mediated effects in tumors

To confirm the importance of CXCL10 in the anti-tumoral effects induced by PAK2 deletion in tumor ECs, neutralizing antibodies against CXCL10 (anti-CXCL10; 50 µg/mouse i.p.) or isotype control IgG2a were administered to CT-PAK2^{EC} or KO-PAK2^{EC} tumor-bearing mice starting on

the fourth day of tumor growth and every three days thereafter during the 18-days growth of LLC tumors (Figure 1A). Similar to Figure 1B, tumors on control IgG2a-treated KO-PAK2^{EC} mice were significantly smaller than tumors on CT-PAK2^{EC} mice (Figure 6A). Notably, tumors on KO-PAK2^{EC} mice treated with anti-CXCL10 grew significantly bigger than tumors on control-treated KO-PAK2^{EC} mice and there was no difference between these and tumors on CT-PAK2^{EC} mice (Figure 6A). Next, we examined if the reduced angiogenesis and vascular normalization observed in KO-PAK2^{EC} tumors were also affected by CXCL10 blockade. The reduction in CD31-content observed in tumors on KO-PAK2^{EC} mice compared to CT-PAK2^{EC} was abolished by the treatment of KO-PAK2^{EC} mice with anti-CXCL10 (Figure 6B, C). Furthermore, there was no difference in CD31 staining levels in tumors from anti-CXCL10-treated KO-PAK2^{EC} mice compared to tumors from CT-PAK2^{EC} mice treated with isotype control (Figure 6B, C). Moreover, CD31-positive vascular structures in these tumors were of smaller diameters (0-10 μm), had decrease pericyte coverage and showed higher fibrinogen leakiness than vascular structures in KO-PAK2^{EC} treated with isotype control as shown by immunostaining indicating that neutralization of CXCL10 in KO-PAK2^{EC} tumors inhibited the vascular normalization induced by PAK2 deletion in tumor ECs (Figure 6D-F).

Finally, the immune cell profiles determined by flow cytometry analyses showed that anti-CXCL10 treatment of KO-PAK2^{EC} mice reduced the amounts of DCs, migratory CD103^{+} DCs, NK cells and of activated CD44^{+} NK cells in tumors (Figure 6G; Figure S5A). Importantly, CXCL10 blockade or endothelial PAK2 deletion in mice did not significantly influence the levels of DCs and NK cells in the spleen (Figure S5B-D). These results confirmed the role of CXCL10 in promoting DCs and NK cells presence in tumors implanted on KO-PAK2^{EC} mice.

Overall, this study demonstrates that CXCL10 produced by ECs of tumors in mice is central for the reduced angiogenesis, vascular normalization, increased infiltration of DCs and NK cells, and the reduced growth of tumors following the inhibition of PAK2 in ECs of tumors.

DISCUSSION

While it was previously known that PAK2 is involved in cellular processes central for angiogenesis (23-25,28,29), the role of PAK2 in tumor blood vessel formation remained ill-defined. Here, we define a non-cell autonomous function of PAK2 in ECs of the TME, which controls tumor angiogenesis and tumor growth. More specifically, PAK2 depletion in tumor ECs decreased tumor vascularization, normalized remaining tumor blood vessels and increased NK cells and DCs infiltration into tumors, leading to reduced tumor growth. Our results indicate a new role for PAK2 in regulating chemokine expression, especially CXCL10. Neutralization of CXCL10 with blocking antibodies reversed the anti-tumor effects induced by PAK2 deletion. Thus, we propose PAK2 inhibition in tumor endothelial cells as an actionable anti-angiogenic therapeutic strategy to improve immunotherapy responses.

We show that blood vessels in KO-PAK2^{EC} tumors were more stable and less permeable than those found in tumors on control mice. Although PAK2-deficient animal models have been linked to hemorrhages and increased vascular permeability (23,30), PAK activation has also been linked to endothelial permeability in various settings. In response to VEGF, thrombotic and inflammatory factors, PAK activation causes EC contraction and pore formation in the endothelial barrier, ultimately leading to vascular permeability (31). PAK activation has also been shown to induce VE-cadherin phosphorylation and internalization, causing a disruption of cell junctions and an increased in permeability to macromolecules in response to VEGF (32). Blocking PAK activity *in vivo* also decreased permeability in animal models of acute lung injury and atherosclerosis (33,34). Therefore, it has been proposed that PAK proteins play various roles in the maintenance of vascular integrity and in the regulation of endothelial permeability in normal and in pathological conditions

(35). Our study supports this position as we demonstrate that deletion of PAK2 in ECs results in reduced vascular permeability and in normalization of tumor blood vessels.

Vascular normalization is generally associated with a boosted immune response in tumors (36). Herein, we show that loss of PAK2 in ECs, in addition to normalizing the tumor vasculature, shifts the TME transcriptome towards a strong innate immune signature and enhances the infiltration of NK cells, activated $CD44^+$ NK cells, DCs and migratory $CD103^+$ DCs into tumors. NK cells exert antitumor effects by their cytotoxic activity towards cancer cells and by the secretion of factors orchestrating the immune response in tumors (37). There is an active crosstalk between NK cells and DCs, which has been shown to promote their activation and maturation, respectively (38). Once mature, DCs adopt migratory properties and traffic to tumor draining lymph nodes to prime T cells against cancer cells (39). Intra-tumoral $CD103^+$ DCs can also re-stimulate cytotoxic T cells directly within the TME (40). Although we did not observe increased T cell infiltration in tumors following PAK2 deletion in tumor ECs, it is possible that T cells found in these tumors are more specific against cancer cells than those found in control tumors due to the increase of DCs in KO-$PAK2^{EC}$ tumors and could also contribute to the reduction of tumor growth along with activated NK cells. Interestingly, presence of NK cells in the TME was shown to correlate with intra-tumoral $CD103^+$ DCs and with the responsiveness to anti-PD-1 immunotherapy in mouse and human cancers (41). This suggests that the increase in these innate immune cells following PAK2 deletion in tumor ECs could be an interesting strategy to improve the response to immunotherapy. The critical role of the tumor immune microenvironment (TIME) in tumor initiation and response to therapy led to the recognition that a better understanding of this process may reveal new therapeutic targets (42). Leveraging our deep RNA-seq data, we uncovered an innate immune component upon

PAK2 deletion in tumor ECs, which we identified as DCs and NK cells, thereby providing genetic evidence for the importance of PAK2 in shaping the TIME.

Our results align with a recent study that demonstrated that PAK4 inhibition in ECs lead to vascular normalization and immune sensibilization in glioblastoma (21), indicating that PAK2 and PAK4 might have overlapping functions in tumor ECs. We did not find in PAK2-depleted ECs any significant change in *PAK4* expression indicating that the effects we observed in KO-PAK2^{EC} tumors are caused specifically by the loss of PAK2. Loss of PAK4 in ECs of glioblastoma resulted in ZEB-1 dependent reprogramming of ECs that affected the expression of cell junction proteins and adhesion molecules that contributed to tumor blood vessel normalization and enhanced T-cell recruitment in tumors. We did not observe an effect of PAK2 loss in ECs on ZEB1 expression indicating that the ZEB1-dependent reprogramming is specific to PAK4 inhibition. Indeed, we identified that the anti-angiogenic and immunogenic effects induced by the deletion of PAK2 are principally mediated by the expression of the chemokine CXCL10 by ECs. We uncovered a previously undocumented role for PAK2 in the regulation of chemokine expression by ECs. We also show that the pharmacological inhibition of PAK2 kinase activity is sufficient to increase CXCL10 levels in ECs. CXCL10 exerts well known immunomodulating and angiostatic effects (14). DCs, NK cells and ECs all express CXCR3, the specific receptor for CXCL10 (43). While CXCL10 induces DC and NK cell chemotaxis (14), binding of CXCL10 to CXCR3 on ECs inhibits endothelial migration and promotes apoptosis (44-46). In addition, CXCL10 can also inhibit endothelial proliferation independently of CXCR3 via the binding to the glycosaminoglycan expressed on EC surface (47,48). We demonstrated that CXCL10 neutralization during tumor growth reversed antitumoral effects mediated by the deletion of PAK2 in tumor ECs in mice. This

demonstrated the importance of CXCL10 in the effects induced by the deletion of PAK2 in ECs of tumors.

There is considerable interest for the development of PAK inhibitors in cancer (49). Our findings demonstrate that PAK2 deletion in tumor ECs results in decreased tumor growth by inhibiting tumor angiogenesis in addition to reversing vascular abnormalities and reducing immune suppression through the expression of CXCL10. We provide insights into the essential role of PAK2 in tumor angiogenesis and report a novel role for PAK2 in regulating CXCL10 expression in tumors. Thus, PAK2 inhibition could be a promising anti-angiogenic target and could potentially improve immunotherapy response, leading to significantly better clinical outcome of many cancer patients.

METHODS

Mice

All animal studies were approved by the Animal Care Committee of the Université de Montréal in agreement with the guidelines established by the Canadian Council on Animal Care. Pak2$^{fl/fl}$ mice were generously provided by Dr. Jonathan Chernoff (Fox Chase Cancer Center) and Pdgfb-iCreER mice were generously provided by Dr. Marcus Fruttiger (University College London). Pdgfb-iCreER;PAK2$^{fl/fl}$ were viable and fertile with no obvious phenotypes. CreER induction and endothelial deletion of PAK2 was achieved by subcutaneous implantation of placebo or tamoxifen slow-release pellets (5 mg/21 days) (Innovative Research of America) into mice neck two days prior tumor implantation.

Cell culture and treatments

Lewis lung carcinoma (LLC) cells obtained from American Type Culture Collection (ATCC) were cultured in Dulbecco modified Eagle medium (DMEM, Thermo Fisher) supplemented with 10% fetal bovine serum (HyClone, GE Healthcare Life Sciences), 2 mM L-glutamine, 100 U/ml penicillin and 100 μg/ml streptomycin (Thermo Fisher). Microvascular mouse lung ECs (MLECs) were isolated from the lungs of Pdgfb-iCre;Pak2$^{fl/fl}$ mice as we previously described (50). MLECs were grown in DMEM:F12 (1:1) medium (Gibco), supplemented with 20% FBS, 0.1 mg/mL heparin (Millipore-Sigma), 100 U/ml penicillin, 100 μg/ml streptomycin and 0.05 mg/mL Endothelial Cell Growth Supplement (ECGS, Corning Life Sciences). Magnetic Dynabeads (Thermo Fisher) were conjugated with anti-mouse CD102 (clone 3C4, BD Biosciences) antibody. Beads were added and incubated for 1h at 4°C. MLECs were selected in a magnetic field for 10 minutes following trypsinization. Isolated MLECs were treated with increasing concentration (0.1, 5 and 50 μM) of 4-hydroxytamoxifen (OH-tamoxifen) (Millipore-Sigma) for 24 h. Human

umbilical vein ECs (HUVECs) obtained from VEC Technologies were cultured in M199 media supplemented with 20% FBS, 2 mM L-glutamine, 100 U/ml penicillin, 100 μg/ml streptomycin and 0.05 mg/mL ECGS. HUVECs were serum starved in M199 media with 0.5% FBS for 3 h followed by a 7 h treatment with 1 μM group I PAK inhibitor FRAX1036 (Selleck Chemicals).

Tumor implantation and monitoring

LLC tumor cells were grown to 80-90% confluence on the day of the implantation. Cells were washed, trypsinized and resuspended in serum, L-glutamine and penicillin/streptomycin-free DMEM. LLC cells (1.5x06 cells in 100 μL) were injected subcutaneously in the flank of 6 to 8 weeks old mice. Tumor volume was determined daily or every other day using a caliper and applying the formula (volume = $0.523 \times (\text{width})^2 \times (\text{length})$) to approximate the volume of a spheroid. When measured every other day, the mean of day before and the day after was used to estimate missing tumor volume. If mice reached ethical end point of experiments before 18 days of tumor growth, tumor volume was estimated using exponential growth equation ($y=y_0*\exp(k*x)$) determined from tumor measures collected prior to euthanasia. Tumor-bearing Pdgfb-iCreER-PAK2$^{fl/fl}$ mice treated with tamoxifen did develop general edema, with an average weight gain of 40% of the mouse's initial weight, without affecting overall survival. Pdgfb-iCreER-PAK2$^{fl/fl}$ mice treated did not develop visible edema.

***In vivo* treatments**

4 days after tumor cells injection ($1.5x10^6$ LLC/100 μL DMEM s.c.), mice were treated with neutralizing anti-CXCL10 antibodies (50μg/100 μL PBS i.p.) every three days for remaining tumor growth time. Tumors were measured daily or every other day, harvested after 18 days of tumor growth.

Immunofluorescence and immunohistochemistry staining and analysis

For immunofluorescence staining, tumors were snap-freeze in liquid nitrogen immediately after resection and embedded in Tissue-Tek OCT (Optimal Cutting temperature) before frozen sectioning on a microtome-cryostat. Tumor sections (7-25 µm) were fixed with 10% formalin-buffered solution (Thermo Fisher) for 10 minutes. 1% bovine serum albumin (BSA)-PBST (phosphate-buffered saline (PBS), 0.5% Triton-X100, 0.02% Tween) was used for permeabilizing and blocking for 1h at room temperature. Slides were incubated overnight at 4°C with primary antibodies (see Antibodies section) in 1% BSA-PBS solution. Fluorescent secondary antibodies were incubated in 1% BSA-PBS solution for 1 h at room temperature before being mounted in Fluoromount G (Electron Microscopy Sciences). Acquisitions were performed on an LSM 800 confocal laser-scanning microscope (Zeiss). Quantifications were performed on ImageJ (National Institute of Health) by applying a threshold on the positive signal level and measuring positive area. For immunofluorescence quantification, 3 to 6 fields (20X) per tumor were scored.

For immunohistochemistry staining, tumors were fixed with 10% formalin-buffered solution (Thermo Fisher) for at least 48 h before being embedded in paraffin. Immunohistochemistry stainings were performed by the Histology Core Facility of the Institute of Research in Immunology and Cancerology of the Université de Montréal (IRIC). Acquisitions were performed on an NanoZoomer 2.0-HT slide scanner (Hamamatsu). Vessel diameters were measured by hand using the NDP.view2 Viewing software (Hamamatsu). For immune cell quantifications and localization, tumors regions were determined manually. Tumor core was defined as highly cellular regions, which consists primarily of tumor cells, and tumor periphery was defined as non-cellular stroma-like regions by analysis of the hematoxylin counterstain. For immunohistochemistry quantification, 6 fields (20X) per tumor were scored.

Tumor mRNA isolation, RNA-seq and analysis

Total mRNA from 3 CT-PAK2^{EC} and 3 KO-PAK2^{EC} average-sized tumors was extracted using TRIZOL reagent (Invitrogen) according to recommended procedures. Total mRNA was cleaned up using RNeasy columns (Qiagen) and on-column DNase I treatment was performed using the RNase-Free DNase set (Qiagen). Tumor mRNA samples were submitted to the Montreal Clinical Research Institute (IRCM) Molecular Biology Core Facility for RNA-sequencing. Sequencing was performed at the Génome Québec Innovation Centre (McGill University) by using the Illumina HiSeq 2000 platform. The quality of the raw reads was assessed with FASTQC version 0.11.8 and combined with MultiQC version 1.3. The reads were aligned to the GRCm38 genome with STAR version 2.5.1b and the raw alignment counts were calculated with featureCounts version 1.6. DESeq2 version 1.24.0 was then used to normalize gene readcounts. A cut-off of >0.5 log2(fold change) and <-0.5 log2(fold change), and an adjusted p-value <0.05 was applied to define differentially expressed genes (DEGs) between KO-PAK2^{EC} and CT-PAK2^{EC} tumors. Bioinformatics analyses were performed using the Database for Annotation, Visualization and Integrated Discovery (version v2023q3, National Institutes of Health) using DEGs, the enrichment of Gene Ontology (GO) categories and Kyoto Encyclopedia of Genes and Genomes (KEGG) pathway were analyzed, and the Gene Set Enrichment Analysis (GSEA) software (version 4.1.0, Broad Institute and University of California San Diego) using all sequenced genes with a base mean over 100 reads.

Flow cytometry experiments

As we previously described (51), mechanical tumor dissociation was done using gentleMACs Dissociator (Miltenyi Biotec) in RPMI media. After centrifugation, red blood cells were lysed with RBC lysis buffer (Gibco) 5 minutes on ice. After PBS wash, cells were marked with FVS-510

viability reagent (BD Bioscience) 15 minutes at room temperature. After 2% FBS/PBS wash, Fc blocking antibodies CD16/CD32 (eBioscience) were incubated for 15 minutes on ice. Brilliant Stain buffer (BD Horizon) and antibodies targeting extracellular proteins were then added and incubated for 30 minutes at room temperature (see Antibodies section). After 2% FBS/PBS wash, cells were either fixed with 2% paraformaldehyde in 2% FBS/PBS solution or stained with antibodies targeting intracellular proteins using the FOXP3/Transcription Factor Staining Buffer set (eBioscience) according to the manufacturer's instructions. For compensation settings, cells and eBeads (eBioscience) were stained with every antibody individually. BD LSR Fortessa and DiVa software (version 8, BD Biosciences) was used for the acquisition and flow cytometry analysis was performed using FlowJo software (version 10, BD Biosciences).

HUVECs transfections

PAK2 small interfering RNA (siRNA) and non-silencing control siRNA were generated by Horizon Discoveries. siCT 5' AUGAACGUGAAUUGCUCAAUU 3', siPAK2 5' UCACCAAACUAGAGCAAAAUU 3' sequences were used. HUVECs were transfected with si-RNAs Lipofectamine 2000 (Thermo Fisher) according to recommended procedures for 48 h to 96 h.

HUVECs mRNA isolation, RNA-seq and analysis

Total mRNA from 3 siCT and 3 siPAK2 independent experiments was extracted using TRIZOL reagent (Invitrogen) according to recommended procedures. Total mRNA was cleaned up using RNeasy columns (Qiagen). HUVEC mRNA samples were submitted to the Institute for Research in Immunology and Cancer (IRIC) Genomics Core Facility. Sequencing was performed at IRIC (Université de Montréal) the by using the Illumina NextSeq500 platform. Quality of the raw reads was assessed with MultiQC version 1.11. Sequences were trimmed for sequencing adapters and

low quality 3' bases using Trimmomatic version 0.35 and aligned to the reference human genome version GRCh38 (gene annotation from Gencode version 37, based on Ensembl 103) using STAR version 2.7.1a. Gene expressions were obtained from STAR both as readcounts and TPM values as well as computed using RSEM in order to obtain normalized gene and transcript level expression, in FPKM and TPM values. DESeq2 version 1.30.1 was then used to normalize gene readcounts. Differential gene expression and bioinformatics analyses were performed as previously described for tumor RNA-seq analysis.

Immunoblotting

HUVECs were solubilized with lysis buffer containing 1% Nonidet P-40, 0.1% sodium dodecyl sulfate (SDS), 0.1% deoxycholic acid, 50 mM Tris–HCl (pH 7.4), 150 mM NaCl, 0.1 mM ethylenediaminetetraacetic acid (EDTA), 0.1 mM ethylene glycol tetraacetic acid (EGTA), 20 mM sodium fluoride, 1 mM sodium pyrophosphate, and 1 mM sodium orthovanadate and Complete mini EDTA free protease inhibitor cocktail (Roche Diagnostics). Soluble proteins were separated by SDS-PAGE, transferred onto a nitrocellulose membrane (Hybond-ECL, GE Healthcare Life Science) and western blotted. Detection and quantification were performed using HRP-coupled secondary antibodies and and an Image Quant LAS4000 chemiluminescence-based detection system (enhanced chemiluminescence) (GE Healthcare Life Science).

Quantitative RT-qPCT validation of RNA-sequencing data

cDNAs were generated from 1 µg off RNA isolated using the SuperScript II Reverse Transcriptase kit for RT-qPCR (Thermo Fisher) according to the manufacturer's instructions. cDNA (0.2 µg) was amplified in quadruplate using PowerUP SYBR Green Master mix (Thermo Fisher). Quantitative real-time PCR (RT-qPCR) was performed with MIC qPCR cycler (Bio Molecular Systems). Gene

expression analysis was performed using the comparative cycle threshold (ΔCT) method, normalized with the expression of reference gene GAPDH.

RT-qPCR Primers

Gene	Primers	Species
SELENBP1	GAAGTCATGGTCAGCACCTT CTTCTCCCATGTCCCTTTCAC	Mouse
MMP2	CCAGATGTGGCCAACTACAA GGTCAGGTGTGTAACCAATGA	Mouse
C1RA	CTTGAATACCCTCAGCCCTATC TCACCCAAGTTCTTCCCATTAG	Mouse
CXCL10	GGCCATAGGGAAGCTTGAAA CAGACATCTCTGCTCATCATTCT	Mouse
ZBP1	CTCCTGCAATCCCTGAGAAC GTCATAGCTCAGAAGGTGCTTAT	Mouse
CASP4	GAAAGAGGAGCTTACAGCAGAG TGAGACATTAGCACCAGGAATG	Mouse
DDX58	CAGAACTGGAACAGGTCGTTTA GCTTCTCTGTCTCCTTCATCAG	Mouse
H2-M3	GCCAGCAGGAACAGTGATTA AGGAGACACAGGTATGGAGAG	Mouse
NOTCH1	GATGGACGACAATCAGAACGA ATCACTCAGGTCAGGGAGAA	Mouse
GAPDH	AACTTTGGCATTGTGGAAGG ACACATTGGGGGTAGGAACA	Mouse
CXCL10	CCATGAATCAAACTGCCATTCT ACTAATGCTGATGCAGGTACA	Human
CX3CL1	CTTACCAGCAGAGCACCTTAG GCTCTGCCCATTTCCATTTG	Human
CXCL11	CAACGATGCCTAAATCCCAAATC GTCCTTTCACCCACCTTTCA	Human
CXCL12	AGAGCCTGAGGGATCTTTACT GGCAGGTACATCCAAGTTCTAC	Human
CCL8	TGGAGAGCTACACAAGAATCAC AGGCTCATGGCTTCAGATTT	Human
CXCL8	GGACAAGAGCCAGGAAGAAA GGGTGGAAAGGTTTGGAGTAT	Human
CXCL1	ACTCAAGAATGGGCGGAAAG	Human

	CTTCTCCTAAGCGATGCTCAAA	
CCL2	CTGTGCCTGCTGCTCATA CTGTGCCTGCTGCTCATA	Human
CXCL3	CTTCTCGCACAGCTTCCC AGACAAGCTTTCTTCCCATTCT	Human
CXCL6	GCTGCGTTGCACTTGTTTAC TCCAGACAAACTTGCTTCCC	Human
CXCL5	CCTGAAGAACGGGAAGGAAA CTGCTGAAGACTGGGAAACT	Human
CXCL2	GCAGGGAATTCACCTCAAGAA TCCTTCTGGTCAGTTGGATTTG	Human
CCL14	AACAGCCAGTGCTCCAAG TGAGAGTTAGCGGTGGGT	Human
GAPDH	CCACTCCTCCACCTTTGAC ACCCTGTTGCTGTAGCCA	Human

Antibodies

Antibodies	**Source**	**Application**
CD31	Biocare Medical 902-303-092017	Immunofluorescence
PAK2	Invitrogen PA5-20254	Immunofluorescence
NG2	Millipore AB5320	Immunofluorescence
Fibrinogen	Dako A0080	Immunofluorescence
CXCL10	Cell Signaling 14969	Immunofluorescence, Immunoblot
CD11c	Cell Signaling 97858	Immunohistochemistry
NK1.1(Klrb1c/CD161c)	Cell Signaling 39197	Immunohistochemistry
CD8	Cell Signaling 98941S	Immunohistochemistry
CD4	Abcam ab183685	Immunohistochemistry
CD8a PerCP-Cy5.5	BD Biosciences 561109	Flow cytometry
CD25 BB515	BD Biosciences 564458	Flow cytometry
CD45 APC-Cy7	BD Biosciences 561037	Flow cytometry
CD19 APC-R700	BD Biosciences 565473	Flow cytometry
CD4 APC	BD Biosciences 561091	Flow cytometry
CD3e BV786	BD Biosciences 564379	Flow cytometry
CD44 BV711	BD Biosciences 563971	Flow cytometry
I-A/I-E BV650	BD Biosciences 563415	Flow cytometry
B220 PE-CF594	BD Biosciences 562313	Flow cytometry
NK1.1 PE-Cy7	BD Biosciences 562062	Flow cytometry
gd TCR PE-Cy7	BD Biosciences 561997	Flow cytometry

Foxp3 PE	eBioscience 48-5773-80	Flow cytometry
CD11b PerCP-Cy5.5	BD Biosciences 561114	Flow cytometry
Ly6G AF700	BD Biosciences 561236	Flow cytometry
CD206 AF647	BD Biosciences 565250	Flow cytometry
CD103 BV786	BD Biosciences 564322	Flow cytometry
F4/80 BV421	BD Biosciences 565411	Flow cytometry
CD11c PE-Cy7	BD Biosciences 561022	Flow cytometry
Ly6C PE-CF594	BD Biosciences 562728	Flow cytometry
CD317 PE	eBioscience 12-3172-81	Flow cytometry
CD19 FITC	BioLegend 115505	Flow cytometry
CD3e FITC	BioLegend 100305	Flow cytometry
NK1.1 FITC	BioLegend 108705	Flow cytometry
PAK2	Cell Signaling 2608	Immunoblot
p-PAK2 (ser141)	Cell Signaling 2606	Immunoblot
HSP90	BD Biosciences 610419	Immunoblot
β-actine	Cell Signaling 3700S	Immunoblot
CXCL10	R&D System MAB466	Neutralization
IgG2a	R&D System MAB006	Neutralization

Statistics

Data are represented as the means ± SEM, except for flow cytometry analysis that are represented as box-and-whisker plot showing median ± minimal to maximal values, from at least 3 independent experiments. Two-tailed independent Student's t tests were used when comparing two groups. Comparison between multiple groups were made using one-way ANOVA or two-way ANOVA followed by post-hoc Tukey's multiple comparison test among groups. For cytometry analyses, outliers were identified and excluded using ROUT method (Q1%). All statistical calculation were performed using GraphPad Prism software (version 10.0.3, Dotmatics). P-value <0.05 was considered statistically significant.

AUTHORS' DISCLOSURES: No disclosures were reported.

AUTHORS' CONTRIBUTIONS: J.C. designed and performed the experiments, analyzed the data, prepared figures, and wrote the manuscript; P.M., C.D and Y.E.B performed experiments, analyzed data and revised the manuscript; M.-A.G. provided key expertise and revised the manuscript; T.H. analyzed data, provided key expertise and revised the manuscript; J.-F.C. obtained funding, designed experiments and revised the manuscript; J.-P.G. obtained funding, designed, and supervised the experiments, analyzed the data, prepared figures, and wrote the manuscript.

ACKNOWLEDMENTS: We thank Eric Massicotte and Julie Lord for their assistance with flow cytometry acquisitions. This work was funded by operating grants from the Cancer Research Society of Canada to J.-P.G. (25151 and 937718), from the Leukemia Lymphoma Society of Canada to T.H., and from the Canadian Institutes of Health Research (CIHR) to J.-F.C. (PJT – 178083), T.H. (PJT – 190275) and J.-P.G (PJT – 180376). J.C. is a recipient of a Fonds de Recherche du Québec – Santé (FRQS) Doctoral training grant. J.-F.C. holds the Canada Research Chair Tier-1 in Cellular Signaling and Cancer Metastasis and the Alain Fontaine Chair in cancer research from the IRCM Foundation. J.-P.G. holds the Merck Canada Chair in Pharmacology from Université de Montréal.

REFERENCES

1. Karin E, Johanna AJ. The evolving tumor microenvironment: From cancer initiation to metastatic outgrowth. Cancer Cell **2023**;41:374-403

2. Folkman J. Tumor angiogenesis: therapeutic implications. N Engl J Med **1971**;285:1182-6

3. Eelen G, Treps L, Li X, Carmeliet P. Basic and Therapeutic Aspects of Angiogenesis Updated. Circ Res **2020**;127:310-29

4. Baeriswyl V, Christofori G. The angiogenic switch in carcinogenesis. Semin Cancer Biol **2009**;19:329-37

5. Pugh CW, Ratcliffe PJ. Regulation of angiogenesis by hypoxia: role of the HIF system. Nature Medicine **2003**;9:677-84

6. Carmeliet P, Jain RK. Angiogenesis in cancer and other diseases. Nature **2000**;407:249-57

7. Siemann DW. The unique characteristics of tumor vasculature and preclinical evidence for its selective disruption by Tumor-Vascular Disrupting Agents. Cancer Treat Rev **2011**;37:63-74

8. Mantovani A, Allavena P, Sica A, Balkwill F. Cancer-related inflammation. Nature **2008**;454:436-44

9. Triner D, Shah YM. Hypoxia-inducible factors: a central link between inflammation and cancer. J Clin Invest **2016**;126:3689-98

10. Ribatti D, Crivellato E. Immune cells and angiogenesis. J Cell Mol Med **2009**;13:2822-33

11. Abdul-Rahman T, Ghosh S, Badar SM, Nazir A, Bamigbade GB, Aji N*, et al.* The paradoxical role of cytokines and chemokines at the tumor microenvironment: a comprehensive review. European Journal of Medical Research **2024**;29:124

12. Mollica Poeta V, Massara M, Capucetti A, Bonecchi R. Chemokines and Chemokine Receptors: New Targets for Cancer Immunotherapy. Frontiers in Immunology **2019**;10

13. Kiefer F, Siekmann AF. The role of chemokines and their receptors in angiogenesis. Cell Mol Life Sci **2011**;68:2811-30

14. Liu M, Guo S, Stiles JK. The emerging role of CXCL10 in cancer (Review). Oncol Lett **2011**;2:583-9

15. Rahma OE, Hodi FS. The Intersection between Tumor Angiogenesis and Immune Suppression. Clinical Cancer Research **2019**;25:5449-57

16. Bergers G, Hanahan D. Modes of resistance to anti-angiogenic therapy. Nature Reviews Cancer **2008**;8:592-603

17. Bokoch GM. Biology of the p21-activated kinases. Annu Rev Biochem **2003**;72:743-81

18. Arias-Romero LE, Chernoff J. A tale of two Paks. Biol Cell **2008**;100:97-108

19. Yurdagul A, Jr., Chen J, Funk SD, Albert P, Kevil CG, Orr AW. Altered nitric oxide production mediates matrix-specific PAK2 and NF-κB activation by flow. Mol Biol Cell **2013**;24:398-408

20. Kelly ML, Chernoff J. Mouse models of PAK function. Cell Logist **2012**;2:84-8

21. Ma W, Wang Y, Zhang R, Yang F, Zhang D, Huang M*, et al.* Targeting PAK4 to reprogram the vascular microenvironment and improve CAR-T immunotherapy for glioblastoma. Nature Cancer **2021**;2:83-97

22. Hofmann C, Shepelev M, Chernoff J. The genetics of Pak. J Cell Sci **2004**;117:4343-54

23. Radu M, Lyle K, Hoeflich KP, Villamar-Cruz O, Koeppen H, Chernoff J. p21-Activated Kinase 2 Regulates Endothelial Development and Function through the Bmk1/Erk5 Pathway. Mol Cell Biol **2015**;35:3990-4005

24. Lamalice L, Houle F, Huot J. Phosphorylation of Tyr1214 within VEGFR-2 triggers the recruitment of Nck and activation of Fyn leading to SAPK2/p38 activation and endothelial cell migration in response to VEGF. J Biol Chem **2006**;281:34009-20

25. Boscher C, Gaonac'h-Lovejoy V, Delisle C, Gratton JP. Polarization and sprouting of endothelial cells by angiopoietin-1 require PAK2 and paxillin-dependent Cdc42 activation. Mol Biol Cell **2019**;30:2227-39

26. Claxton S, Kostourou V, Jadeja S, Chambon P, Hodivala-Dilke K, Fruttiger M. Efficient, inducible Cre-recombinase activation in vascular endothelium. Genesis **2008**;46:74-80

27. Ong CC, Gierke S, Pitt C, Sagolla M, Cheng CK, Zhou W*, et al.* Small molecule inhibition of group I p21-activated kinases in breast cancer induces apoptosis and potentiates the activity of microtubule stabilizing agents. Breast Cancer Res **2015**;17:59

28. Koh W, Mahan RD, Davis GE. Cdc42- and Rac1-mediated endothelial lumen formation requires Pak2, Pak4 and Par3, and PKC-dependent signaling. J Cell Sci **2008**;121:989-1001

29. Koh W, Sachidanandam K, Stratman AN, Sacharidou A, Mayo AM, Murphy EA*, et al.* Formation of endothelial lumens requires a coordinated PKCepsilon-, Src-, Pak- and Raf-kinase-dependent signaling cascade downstream of Cdc42 activation. J Cell Sci **2009**;122:1812-22

30. Buchner DA, Su F, Yamaoka JS, Kamei M, Shavit JA, Barthel LK*, et al.* pak2a mutations cause cerebral hemorrhage in redhead zebrafish. Proc Natl Acad Sci U S A **2007**;104:13996-4001

31. Stockton RA, Schaefer E, Schwartz MA. p21-activated kinase regulates endothelial permeability through modulation of contractility. J Biol Chem **2004**;279:46621-30

32. Gavard J, Gutkind JS. VEGF controls endothelial-cell permeability by promoting the beta-arrestin-dependent endocytosis of VE-cadherin. Nat Cell Biol **2006**;8:1223-34

33. Stockton R, Reutershan J, Scott D, Sanders J, Ley K, Schwartz MA. Induction of vascular permeability: beta PIX and GIT1 scaffold the activation of extracellular signal-regulated kinase by PAK. Mol Biol Cell **2007**;18:2346-55

34. Orr AW, Stockton R, Simmers MB, Sanders JM, Sarembock IJ, Blackman BR*, et al.* Matrix-specific p21-activated kinase activation regulates vascular permeability in atherogenesis. J Cell Biol **2007**;176:719-27

35. Galan Moya EM, Le Guelte A, Gavard J. PAKing up to the endothelium. Cell Signal **2009**;21:1727-37

36. Magnussen AL, Mills IG. Vascular normalisation as the stepping stone into tumour microenvironment transformation. Br J Cancer **2021**;125:324-36

37. Wolf NK, Kissiov DU, Raulet DH. Roles of natural killer cells in immunity to cancer, and applications to immunotherapy. Nature Reviews Immunology **2023**;23:90-105

38. Walzer T, Dalod M, Robbins SH, Zitvogel L, Vivier E. Natural-killer cells and dendritic cells: "l'union fait la force". Blood **2005**;106:2252-8

39. Liu J, Zhang X, Cheng Y, Cao X. Dendritic cell migration in inflammation and immunity. Cellular & Molecular Immunology **2021**;18:2461-71

40. Broz Miranda L, Binnewies M, Boldajipour B, Nelson Amanda E, Pollack Joshua L, Erle David J*, et al.* Dissecting the Tumor Myeloid Compartment Reveals Rare Activating Antigen-Presenting Cells Critical for T Cell Immunity. Cancer Cell **2014**;26:638-52

41. Barry KC, Hsu J, Broz ML, Cueto FJ, Binnewies M, Combes AJ*, et al.* A natural killer-dendritic cell axis defines checkpoint therapy-responsive tumor microenvironments. Nat Med **2018**;24:1178-91

42. Binnewies M, Roberts EW, Kersten K, Chan V, Fearon DF, Merad M*, et al.* Understanding the tumor immune microenvironment (TIME) for effective therapy. Nat Med **2018**;24:541-50

43. García-López MA, Sánchez-Madrid F, Rodríguez-Frade JM, Mellado M, Acevedo A, García MI*, et al.* CXCR3 chemokine receptor distribution in normal and inflamed tissues: expression on activated lymphocytes, endothelial cells, and dendritic cells. Lab Invest **2001**;81:409-18

44. Lasagni L, Francalanci M, Annunziato F, Lazzeri E, Giannini S, Cosmi L*, et al.* An alternatively spliced variant of CXCR3 mediates the inhibition of endothelial cell growth induced by IP-10, Mig, and I-TAC, and acts as functional receptor for platelet factor 4. J Exp Med **2003**;197:1537-49

45. Yates-Binder CC, Rodgers M, Jaynes J, Wells A, Bodnar RJ, Turner T. An IP-10 (CXCL10)-derived peptide inhibits angiogenesis. PLoS One **2012**;7:e40812

46. Bodnar RJ, Yates CC, Wells A. IP-10 blocks vascular endothelial growth factor-induced endothelial cell motility and tube formation via inhibition of calpain. Circ Res **2006**;98:617-25

47. Campanella GS, Colvin RA, Luster AD. CXCL10 can inhibit endothelial cell proliferation independently of CXCR3. PLoS One **2010**;5:e12700

48. Luster AD, Greenberg SM, Leder P. The IP-10 chemokine binds to a specific cell surface heparan sulfate site shared with platelet factor 4 and inhibits endothelial cell proliferation. J Exp Med **1995**;182:219-31

49. Radu M, Semenova G, Kosoff R, Chernoff J. PAK signalling during the development and progression of cancer. Nature Reviews Cancer **2014**;14:13-25

50. Smith TL, Oubaha M, Cagnone G, Boscher C, Kim JS, El Bakkouri Y*, et al.* eNOS controls angiogenic sprouting and retinal neovascularization through the regulation of endothelial cell polarity. Cellular and Molecular Life Sciences **2021**;79:37

51. Goyette MA, Elkholi IE, Apcher C, Kuasne H, Rothlin CV, Muller WJ*, et al.* Targeting Axl favors an antitumorigenic microenvironment that enhances immunotherapy responses by decreasing Hif-1α levels. Proc Natl Acad Sci U S A **2021**;118

FIGURE LEGENDS

Figure 1. Deletion of PAK2 in tumor ECs inhibits tumor angiogenesis, leading to reduced tumor growth and normalized tumor vasculature. (A) Schematic illustration of cohort experiments performed on 6 to 8 weeks old mice. Mice were treated with placebo or tamoxifen (TAM; slow-release pellet, 5 mg/21 days s.c.) and injected with $1.5x10^6$ Lewis lung carcinoma (LLC) cells (s.c.). **(B)** Tumor growth curves of LLC tumors implanted on PCB-PAK2^{EC} (n=14 mice), CT-PAK2^{EC} (n=31 mice) and KO-PAK2^{EC} mice (n=31 mice). *p<0.05 between CT-PAK2^{EC} and KO-PAK2^{EC}, #p<0.05 between PCB-PAK2^{EC} and KO-PAK2^{EC}. **(C)** Visualization of the endothelial-cell specific deletion of PAK2 in tumor. Scale = 20 μm. **(D)** Representative images of CD31$^+$ staining in tumors sections. Scale = 50 μm. **(E)** Quantification of CD31$^+$ vascular area in tumors (CD31$^+$ area/total area) (n=6 tumors). **(F)** Quantification of diameters of CD31$^+$ vascular structures in tumors (n=6 tumors). **(G)** Quantification of NG2$^+$ pericyte coverage of blood vessels in tumors (NG2$^+$ area /CD31$^+$ area) (n=6 tumors). Scale = 20 μm. **(H)** Quantification of Fibrinogen leakage from blood vessels in tumors (Fibrinogen$^+$ area/CD31$^+$ area) (n=5-6 tumors). Scale = 20 μm. All data are represented as mean ± SEM. *p<0.05, **p<0.01.

Figure 2. Tumor endothelial-specific deletion of PAK2 reprograms the immune response gene expression in the tumor microenvironment. (A) Volcano plot showing DEGs in red circles (644 genes) between KO-PAK2^{EC} (n=3 tumors) and CT-PAK2^{EC} (n=3 tumors) from bulk RNA-seq. A threshold of a $\log_2$(Fold Change) >0.5 and <-0.5, and a p-adjusted value <0.05 was used to define DEGs. **(B)** Bar chart of the top 20 significant GO terms of DEGs submitted to the DAVID database and categorized using the biological process annotations. The x-axis indicates the statistical

significance of the enrichment (-$\log_{10}$(FDR)). Color-coding indicates the gene ratio, referencing to the ratio of DEGs annotated in the given GO term to all genes annotated in the GO term. **(C-D)** GSEA of GO terms (C) immune response (GO:0006955) and (D) sprouting angiogenesis (GO:0002040) of KO-PAK2EC compared to CT-PAK2EC tumor gene expression. Heatmaps represent the top 10 genes contributing to the normalized enrichment score (NES). **(E)** Bar chart of selected GO terms of DEGs submitted to the DAVID database and categorized using the biological process annotations related to cytokine response, cell adhesion and cell chemotaxis. The x-axis indicates the statistical significance of the enrichment (-$\log_{10}$(FDR)). Color-coding indicates the gene ratio, referencing to the ratio of DEGs annotated in the given GO term to all genes annotated in the GO term. **(F-G)** GSEA of GO terms (F) GO term leukocyte cell-cell adhesion (GO:0007159) and (G) leukocyte chemotaxis (GO:0030595) of KO-PAK2^{EC} compared to CT-PAK2^{EC} tumor gene expression. Heatmaps represent the top 10 genes contributing to the NES. The scale for Z scores in the heatmaps of panels F-H is shown in panel C.

Figure 3. Deletion of PAK2 in ECs of tumors favors innate immune cell infiltration. (A) Flow cytometry analysis of immune cell infiltration into KO-PAK2^{EC} tumors relative to CT-PAK2^{EC} tumors (n=10-12 tumors). DCs (CD45^{+}I-A/I-E^{+}CD11c^{+}), migratory CD103^{+} DCs, NK cells (CD45^{+}CD8^{-}CD4^{-}NK1.1^{+}) and activated CD44+ NK cells are enriched in KO-PAK2^{EC}. The number of immune cells for each population was normalized to the number of total live cells. Combined data of three independent experiments are shown and represented as median ± minimal to maximal values. *$p<0.05$. **(B-E)** Immunohistochemistry analysis of KO-PAK2^{EC} and CT-PAK2^{EC} tumors. Quantification of DCs (CD11c^{+}) in the (B) core regions and (C) periphery of

tumors (n=5-6 tumors). Quantification of NK cells ($NK1.1^+$) in the (D) core regions and (E) periphery of tumors (n=5-6 tumors). Data are represented as mean ± SEM. *p<0.05.

Figure 4. PAK2 downregulation in ECs increases the expression of CXCL10. (A) Volcano plot showing DEGs in red circles (1,521 genes) between siPAK2 (n=3) and siCT (n=3) transfected HUVECs from bulk RNA-seq. A threshold of a $\log_2$(Fold Change) >0.5 and <-0.5, and a p-adjusted value <0.05 was used to define DEGs. **(B)** Heatmap of the top 20 upregulated DEGs in siPAK2 compared to siCT transfected HUVECs. **(C)** GSEA of GO term chemokine production (GO:0032602). Heatmaps represent the top 10 genes contributing to the normalized enrichment score (NES). The scale for Z scores in the heatmaps of panel C is shown in panel B. **(D)** Heatmap of the chemokine DEGs in siPAK2 compared to siCT transfected HUVECs. **(E)** Expression of chemokines genes measured by RT-qPCR, normalized to GAPDH housekeeping gene, expressed as fold change of siPAK2 relative to siCT transfected HUVECs. **(F)** Expression of CXCL10 gene measured by RT-qPCR, normalized to GAPDH housekeeping gene and expressed as fold change of FRAX1036 treated HUVECs relative to non-treated HUVECs. PAK2 inhibition was monitored by Western blot analysis following FRAX1036 treatment (1 μM). β-actin served as loading control. **(G)** Protein expression of CXCL10 in cell supernatant and cell lysate in siPAK2 and siCT transfected HUVECs. PAK2 downregulation was monitored in siPAK2 transfected cells, and Ponceau S staining and β-actin served as loading control for cell supernatant and cell lysate respectively. *p<0.05. **p<0.01. Data are represented as mean ± SEM.

Figure 5. Deletion of PAK2 in tumor ECs enhances CXCL10 expression in tumors. (A) Fold change expression of the chemokine DEGs in KO-PAK2^{EC} compared to CT-PAK2^{EC} tumors. **(B)** Visualization of CXCL10^{+} clusters relative to CD31^{+} vascular structures in tumors. **(C)** Quantification of CXCL10^{+} area in tumor sections (CXCL10^{+} area/total area) (n=4-5 tumors). **(D)** Quantification of the distance of CXCL10^{+} clusters from CD31^{+} vascular structures in tumors (n=4-5 tumors). *p<0.05. Data are represented as mean ± SEM.

Figure 6. Neutralization of CXCL10 reverses the effects of endothelial-specific deletion of PAK2 on tumor growth, tumor angiogenesis and immune-sensibilization of tumors. (A) Tumor growth curves of LLC tumors implanted on CT-PAK2^{EC} (n=18 mice) and KO-PAK2^{EC} mice (n=13 mice) treated with control IgG2a isotype, and KO-PAK2^{EC} mice (n=14 mice) treated with CXCL10-neutralizing antibodies (anti-CXCL10, 50 μg i.p.). Arrows indicate time of isotype or antibodies injections. *p<0.05 between CT-PAK2^{EC} control-treated and KO-PAK2^{EC} control-treated mice, #p<0.05 between KO-PAK2^{EC} control-treated and KO-PAK2^{EC} anti-CXCL10 treated mice. **(B)** Representative images of CD31^{+} staining in tumors sections. Scale = 50 μm. **(C)** Quantification of CD31^{+} vascular area in tumors (CD31^{+} area/total area) (n=6 tumors). **(D)** Quantification of diameters of CD31^{+} vascular structures in tumors (n=6 tumors). **€** Quantification of NG2^{+} pericyte coverage of blood vessels in tumors (NG2^{+} area/CD31^{+} area) (n=6 tumors). Scale = 20 μm. **(F)** Quantification of Fibrinogen leakage from blood vessels in tumors (Fibrinogen^{+} area/CD31^{+} area) (n=5-6 tumors). Scale = 20 μm. **(G)** Flow cytometry analysis of DCs and NK cells infiltration into KO-PAK2^{EC} control-treated and KO-PAK2^{EC} anti-CXCL10 treated tumors, relative to CT-PAK2^{EC} control-treated tumors (n=6-13 tumors). The number of immune cells for each population was normalized to the number of total live cells. Combined data of three

independent experiments are shown. (A-F) data are represented as mean ± SEM, and (G) data are represented as median ± minimal to maximal values. *$p<0.05$, **$p<0.01$, ***$p<0.001$.

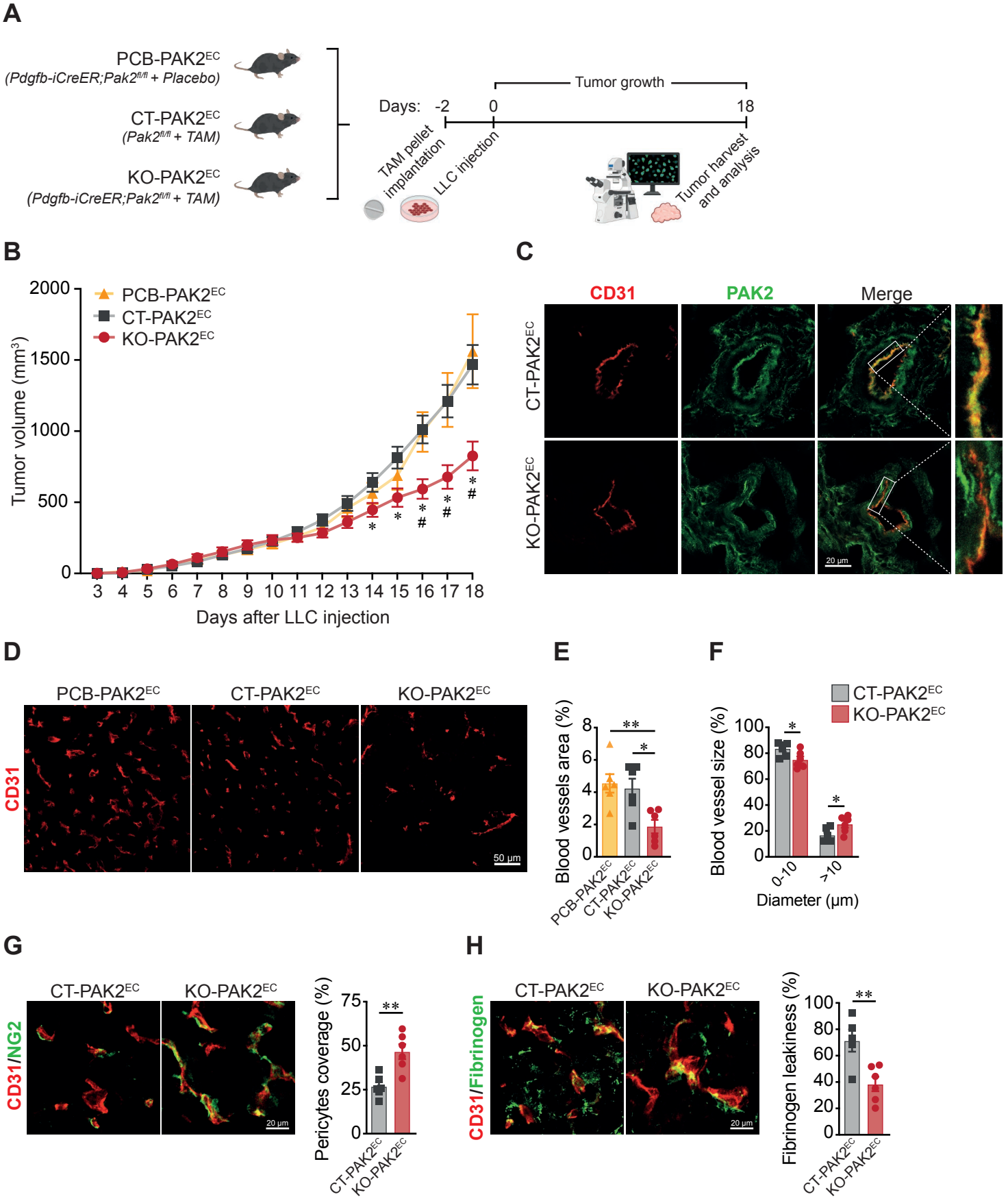
A
PCB-PAK2EC
(Pdgfb-iCreER;Pak2fl/fl + Placebo)
CT-PAK2EC
(Pak2fl/fl + TAM)
KO-PAK2EC
(Pdgfb-iCreER;Pak2fl/fl + TAM)
Tumor growth
Days: -2 0 18
TAM pellet implantation
LLC injection
Tumor harvest and analysis
B
PCB-PAK2EC
CT-PAK2EC
KO-PAK2EC
Tumor volume (mm3)
Days after LLC injection
C
CD31
PAK2
Merge
CT-PAK2EC
KO-PAK2EC
20 µm
D
PCB-PAK2EC
CT-PAK2EC
KO-PAK2EC
CD31
50 µm
E
Blood vessels area (%)
PCB-PAK2EC
CT-PAK2EC
KO-PAK2EC
F
CT-PAK2EC
KO-PAK2EC
Blood vessel size (%)
0-10
>10
Diameter (µm)
G
CT-PAK2EC
KO-PAK2EC
CD31/NG2
20 µm
Pericytes coverage (%)
H
CT-PAK2EC
KO-PAK2EC
CD31/Fibrinogen
20 µm
Fibrinogen leakiness (%)

Figure 1.

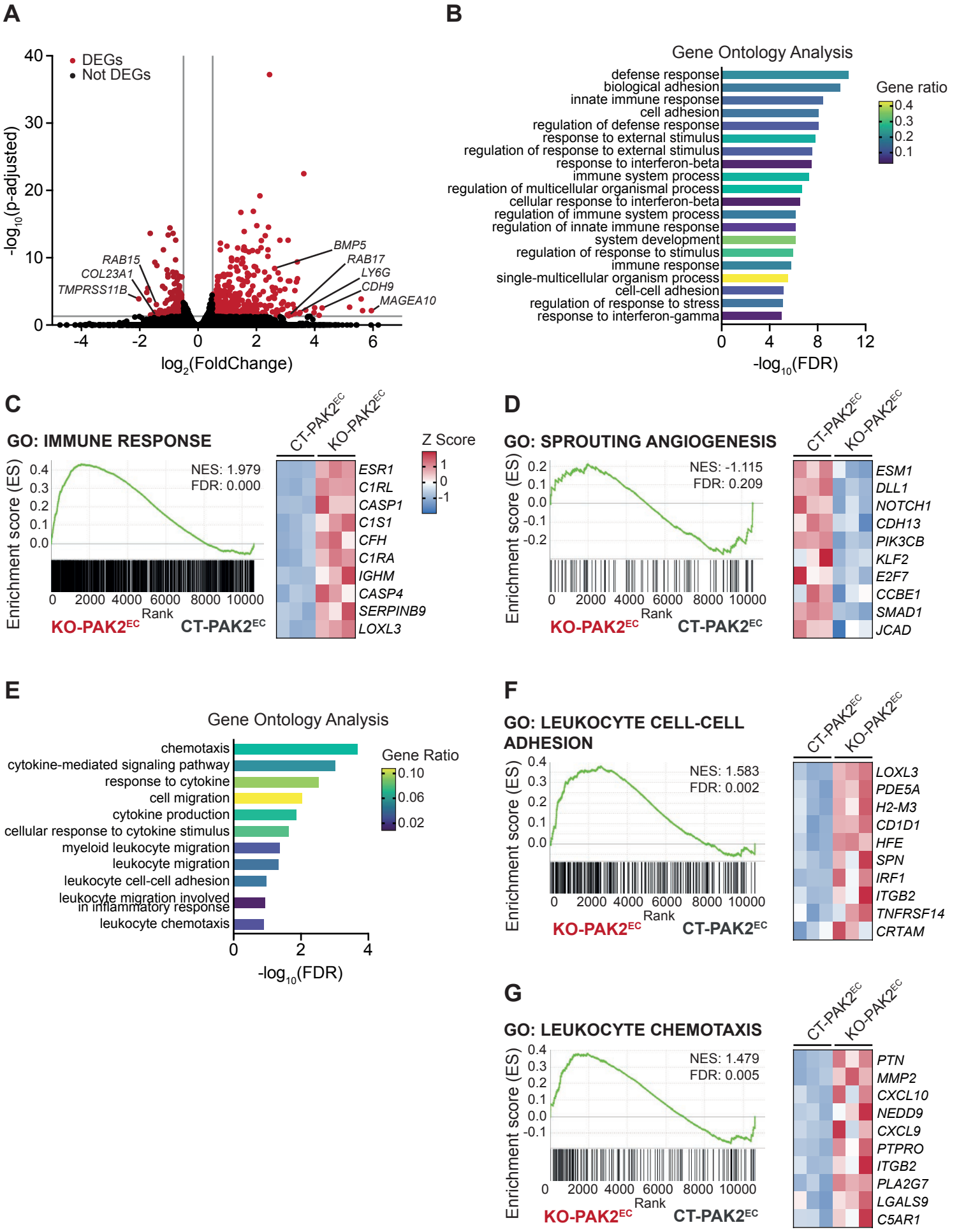
A
DEGs
Not DEGs
-log10(p-adjusted)
log2(FoldChange)
RAB15
COL23A1
TMPRSS11B
BMP5
RAB17
LY6G
CDH9
MAGEA10
B
Gene Ontology Analysis
defense response
biological adhesion
innate immune response
cell adhesion
regulation of defense response
response to external stimulus
regulation of response to external stimulus
response to interferon-beta
immune system process
regulation of multicellular organismal process
cellular response to interferon-beta
regulation of immune system process
regulation of innate immune response
system development
regulation of response to stimulus
immune response
single-multicellular organism process
cell-cell adhesion
regulation of response to stress
response to interferon-gamma
Gene ratio
-log10(FDR)
C
GO: IMMUNE RESPONSE
NES: 1.979
FDR: 0.000
Enrichment score (ES)
Rank
KO-PAK2EC
CT-PAK2EC
Z Score
ESR1
C1RL
CASP1
C1S1
CFH
C1RA
IGHM
CASP4
SERPINB9
LOXL3
D
GO: SPROUTING ANGIOGENESIS
NES: -1.115
FDR: 0.209
ESM1
DLL1
NOTCH1
CDH13
PIK3CB
KLF2
E2F7
CCBE1
SMAD1
JCAD
E
Gene Ontology Analysis
chemotaxis
cytokine-mediated signaling pathway
response to cytokine
cell migration
cytokine production
cellular response to cytokine stimulus
myeloid leukocyte migration
leukocyte migration
leukocyte cell-cell adhesion
leukocyte migration involved in inflammatory response
leukocyte chemotaxis
Gene Ratio
-log10(FDR)
F
GO: LEUKOCYTE CELL-CELL ADHESION
NES: 1.583
FDR: 0.002
LOXL3
PDE5A
H2-M3
CD1D1
HFE
SPN
IRF1
ITGB2
TNFRSF14
CRTAM
G
GO: LEUKOCYTE CHEMOTAXIS
NES: 1.479
FDR: 0.005
PTN
MMP2
CXCL10
NEDD9
CXCL9
PTPRO
ITGB2
PLA2G7
LGALS9
C5AR1

Figure 2.

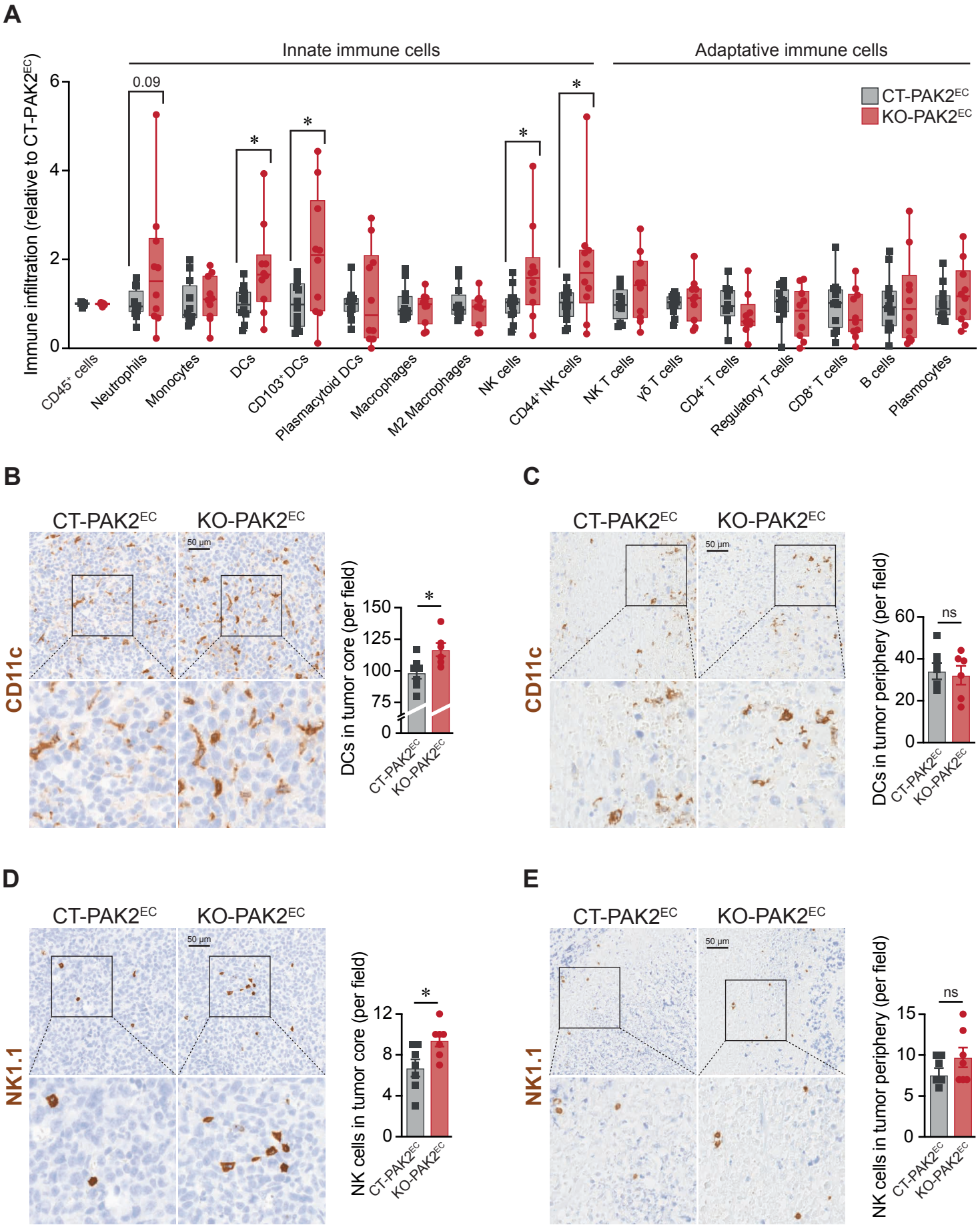
A
Innate immune cells
Adaptative immune cells
Immune infiltration (relative to CT-PAK2EC)
CT-PAK2EC
KO-PAK2EC
0.09
*
CD45+ cells
Neutrophils
Monocytes
DCs
CD103+ DCs
Plasmacytoid DCs
Macrophages
M2 Macrophages
NK cells
CD44+ NK cells
NK T cells
γδ T cells
CD4+ T cells
Regulatory T cells
CD8+ T cells
B cells
Plasmocytes
B
C
D
E
CD11c
NK1.1
50 µm
DCs in tumor core (per field)
DCs in tumor periphery (per field)
NK cells in tumor core (per field)
NK cells in tumor periphery (per field)
ns

Figure 3.

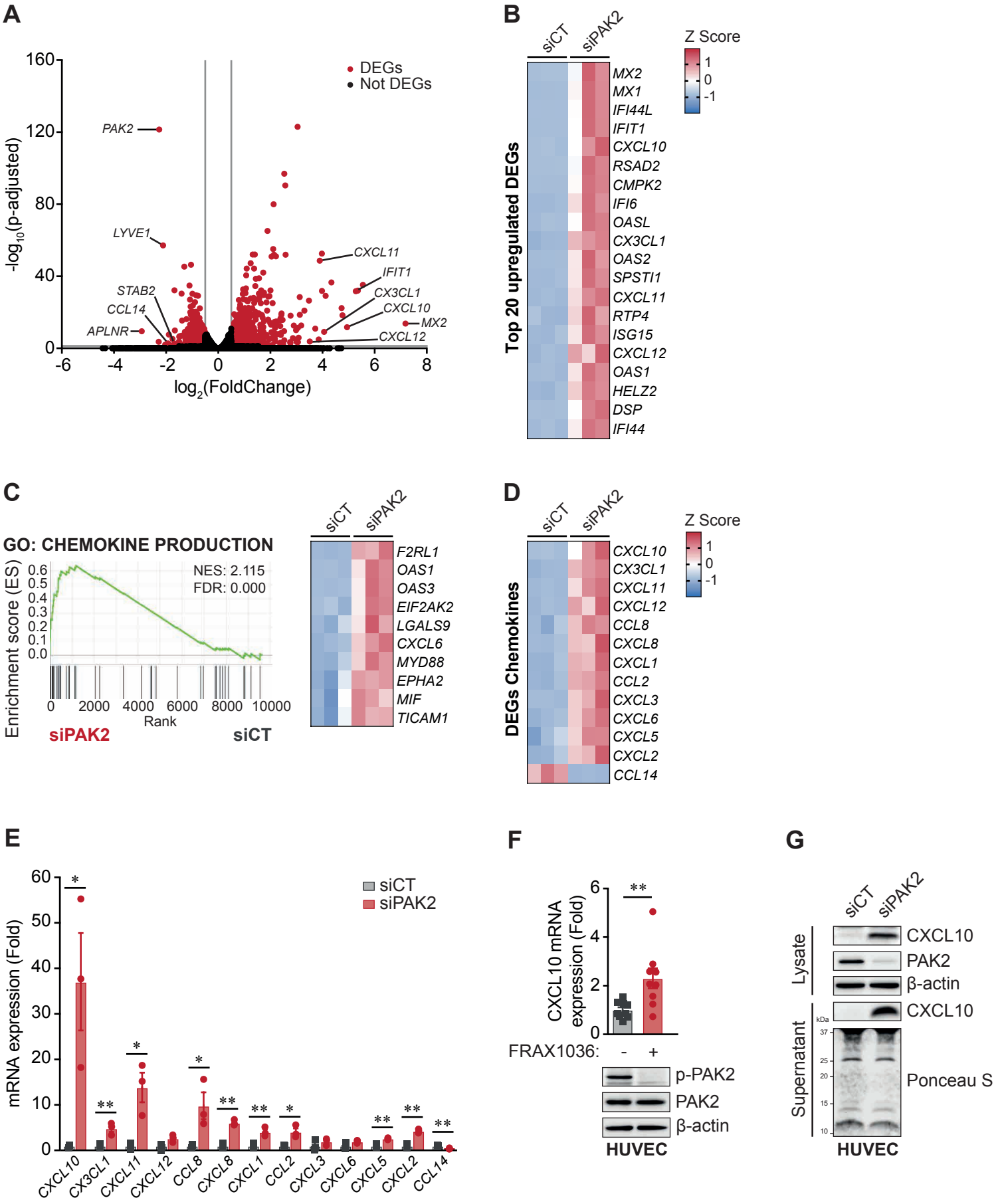
A
DEGs
Not DEGs
PAK2
LYVE1
STAB2
CCL14
APLNR
CXCL11
IFIT1
CX3CL1
CXCL10
MX2
CXCL12
-log10(p-adjusted)
log2(FoldChange)
B
siCT
siPAK2
Z Score
Top 20 upregulated DEGs
MX2
MX1
IFI44L
IFIT1
CXCL10
RSAD2
CMPK2
IFI6
OASL
CX3CL1
OAS2
SPSTI1
CXCL11
RTP4
ISG15
CXCL12
OAS1
HELZ2
DSP
IFI44
C
GO: CHEMOKINE PRODUCTION
NES: 2.115
FDR: 0.000
Enrichment score (ES)
Rank
siPAK2
siCT
F2RL1
OAS1
OAS3
EIF2AK2
LGALS9
CXCL6
MYD88
EPHA2
MIF
TICAM1
D
DEGs Chemokines
CXCL10
CX3CL1
CXCL11
CXCL12
CCL8
CXCL8
CXCL1
CCL2
CXCL3
CXCL6
CXCL5
CXCL2
CCL14
E
siCT
siPAK2
mRNA expression (Fold)
CXCL10
CX3CL1
CXCL11
CXCL12
CCL8
CXCL8
CXCL1
CCL2
CXCL3
CXCL6
CXCL5
CXCL2
CCL14
F
CXCL10 mRNA expression (Fold)
FRAX1036:
-
+
p-PAK2
PAK2
β-actin
HUVEC
G
siCT
siPAK2
Lysate
CXCL10
PAK2
β-actin
Supernatant
CXCL10
Ponceau S
HUVEC

Figure 4.

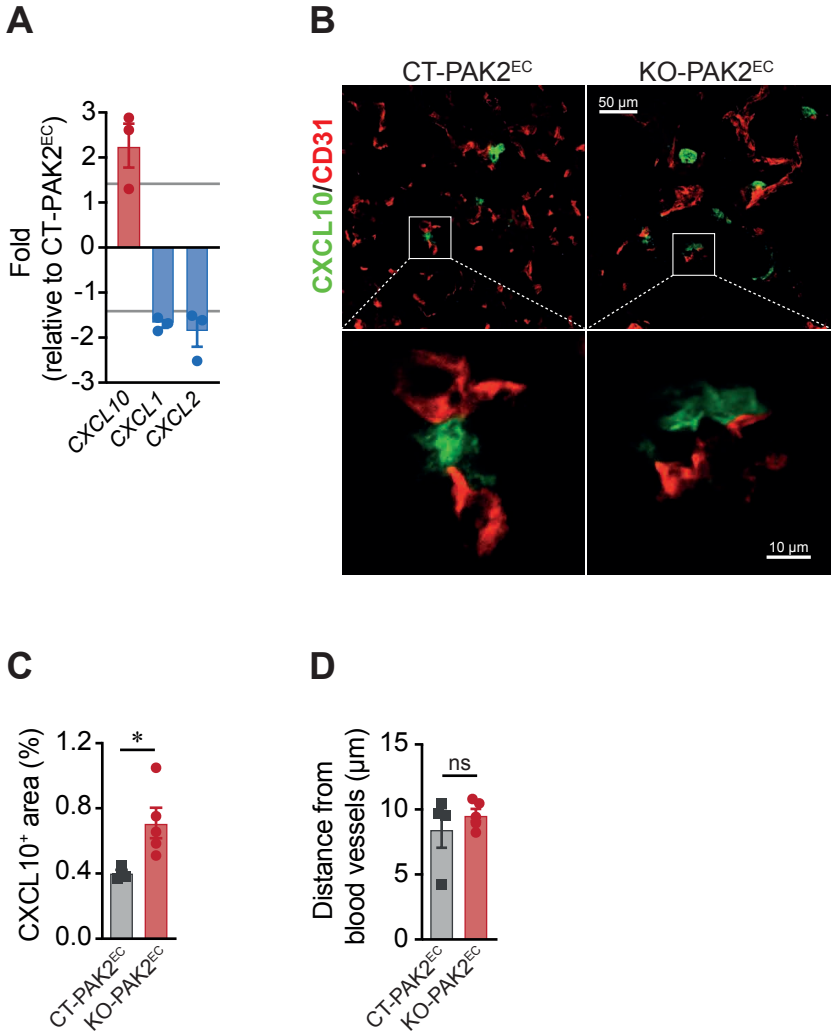
A
Fold
(relative to CT-PAK2EC)
3
2
1
0
-1
-2
-3
CXCL10
CXCL1
CXCL2
B
CT-PAK2EC
KO-PAK2EC
CXCL10/CD31
50 µm
10 µm
C
CXCL10+ area (%)
1.2
0.8
0.4
0.0
*
CT-PAK2EC
KO-PAK2EC
D
Distance from
blood vessels (µm)
15
10
5
0
ns
CT-PAK2EC
KO-PAK2EC

Figure 5.

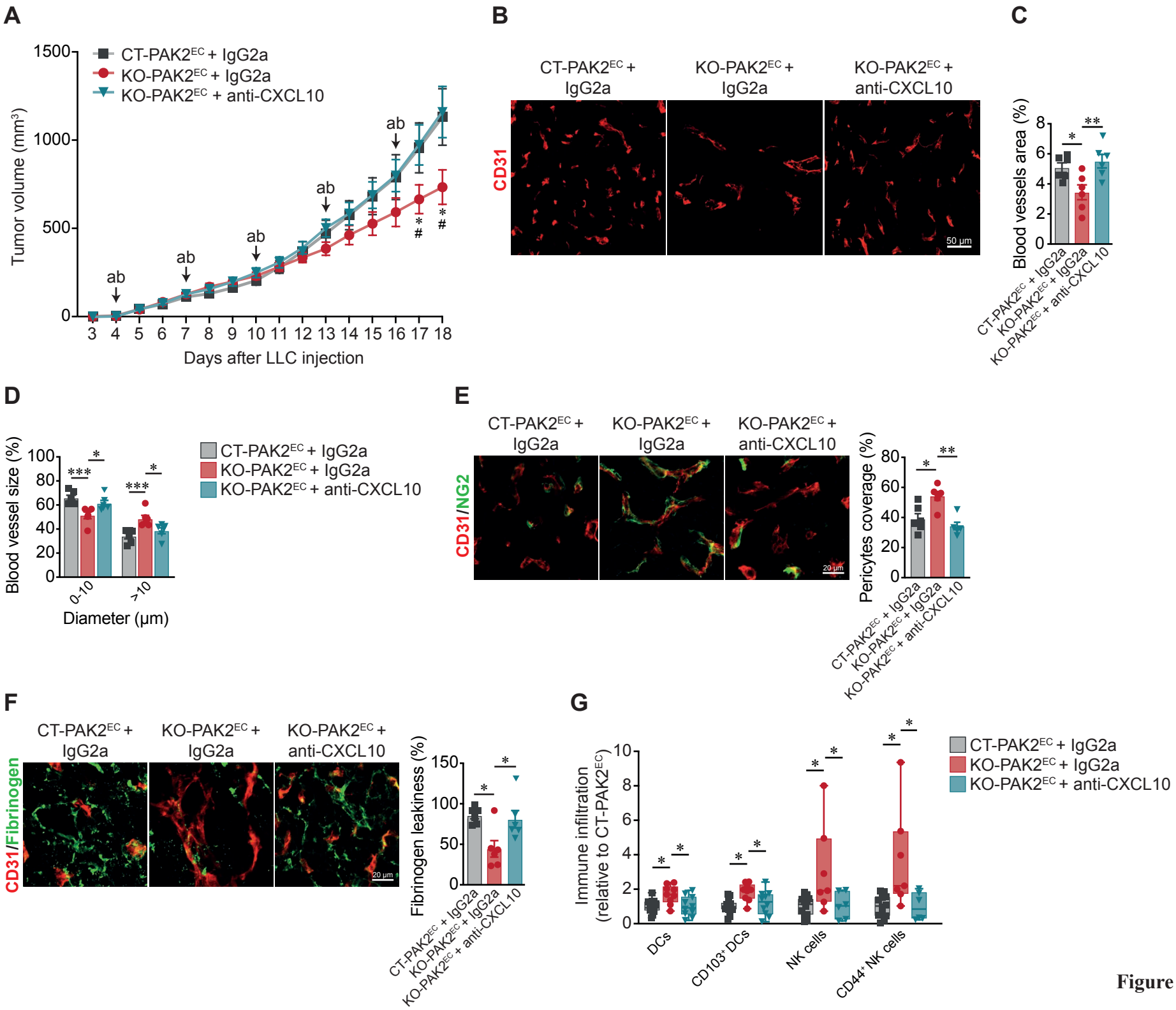
A
CT-PAK2EC + IgG2a
KO-PAK2EC + IgG2a
KO-PAK2EC + anti-CXCL10
Tumor volume (mm3)
Days after LLC injection
ab
B
CT-PAK2EC + IgG2a
KO-PAK2EC + IgG2a
KO-PAK2EC + anti-CXCL10
CD31
50 µm
C
Blood vessels area (%)
D
Blood vessel size (%)
Diameter (µm)
0-10
>10
E
CD31/NG2
20 µm
Pericytes coverage (%)
F
CD31/Fibrinogen
20 µm
Fibrinogen leakiness (%)
G
Immune infiltration (relative to CT-PAK2EC)
DCs
CD103+ DCs
NK cells
CD44+ NK cells

Figure 6.